

The influence of nuclei content on cloud cavitation about a hydrofoil

James Venning^{1*}, Samuel Smith¹, Paul Brandner¹, Dean Giosio¹, Bryce Pearce¹



ISROMAC 2017

International
Symposium on
Transport Phenomena
and
Dynamics of Rotating
Machinery

Maui, Hawaii

December 16-21, 2017

Abstract

The dynamics of cloud cavitation about a 3D hydrofoil are investigated experimentally in a cavitation tunnel with both an abundance and dearth of freestream nuclei. The rectangular-planform, NACA 0015 hydrofoil was tested at a Reynolds number of 1.4×10^6 , a cavitation number of 0.55 and an incidence of 6° . High-speed photography of cavitation shedding phenomena was acquired simultaneously with unsteady force measurement to enable identification of cavity shedding modes corresponding with force spectral peaks. Two shedding modes are evident for both the nuclei deplete and abundant cases, although each are driven by different flow phenomena. The high-frequency mode for the nuclei deplete case is driven primarily by large-scale re-entrant jet formation during the growth phase, but shockwave propagation for the collapse phase of the cycle. The weaker low-frequency mode occurs because the strength of shedding at the hydrofoil tip varies at half the fundamental frequency. The dominant mode for the abundant case is the low-frequency mode which is some 1.8 times slower than the nuclei deplete case. The high-frequency mode for the nuclei abundant case is due to the propagation of two shockwaves; the passage of the first only partially condenses the cavity, while the second condenses a much larger region of the cavity.

Keywords

Cavitation – Nucleation – Hydrofoils – Cavity dynamics

¹ Cavitation Research Laboratory, Australian Maritime College, Launceston, Australia

*Corresponding author: mail@jamesvenning.net

1. INTRODUCTION

The random or periodic formation, separation and collapse of sheet cavities (i.e. partial cavitation) is generally described as cloud cavitation. For sufficiently thick cavities the re-entrant jet, stemming from the cavity closure, has sufficient intensity to grow upstream and impinge upon the cavity interface, detaching a portion that condenses to a bubble cloud and is entrained downstream by the overlying flow [1]. This phenomenon has been widely studied in various contexts including hydrofoils [2, 3, 4, 5], rotating machinery [6, 7], nozzles/venturies [8, 9, 10, 11], wall-mounted cavitators [12] and bluff bodies [13, 14, 15]. Recently it has been shown that the formation of condensation shockwaves produce another instability mechanism for partial cavitation, either singularly or coupled with a re-entrant jet [16, 17]. Three-dimensional flow features have been shown to significantly alter the re-entrant flow topology and the resulting shedding physics [18, 19, 20]. The present work has also observed that the three-dimensional nature of a cavitating flow alters the shockwave behaviour if present.

Inception of hydrodynamic cavitation in practical flows is invariably due to heterogeneous nucleation. These discrete sites of weakness, termed nuclei, are typically microbubbles either free in the liquid volume, or volumes of gas trapped in or on adjacent surfaces. Nuclei have been shown to control not only inception [21] but also the dynamics of cavitation [22]. The water tunnel at the Australian Maritime College has been specifically designed to control the free microbubble content serving as free nuclei in the test water and has the

capacity to investigate the effect of varying nuclei content on cavitating flows. In the present work a preliminary study has been undertaken on the effect of nuclei content on cloud cavitation about a finite span hydrofoil and results are presented for two cases: nuclei deplete water and water seeded with a high nuclei concentration (referred to as the abundant case), maintaining all other flow conditions.

2. EXPERIMENTAL OVERVIEW

Experiments were carried out in the Cavitation Research Laboratory (CRL) variable pressure water tunnel at the Australian Maritime College (AMC). The tunnel test section (figure 1) is 0.6 m square by 2.6 m long in which the operating velocity and absolute pressure ranges are 2 to 12 m/s and 4 to 400 kPa respectively. The tunnel volume is 365 m³ with demineralised water as the working fluid. The CRL tunnel has ancillary systems for rapid degassing and for continuous injection and removal of cavitation nuclei and large volumes of incondensable gas. Further description of the facility is given in [23].

The model hydrofoil of anodised aluminium has a rectangular planform of 0.3 m span and 0.15 m chord with constant NACA 0015 section and a faired tip. The model is mounted vertically from the test section ceiling on a 6-component force balance for dynamic force measurement.

Measurements were made at a cavitation number of 0.55 and a Reynolds number (based on chord length) of 1.4×10^6 with the hydrofoil set at a fixed incidence of 6° . The cavitation number is defined as $\sigma = 2(p_\infty - p_v)/\rho U_\infty^2$ and Reynolds

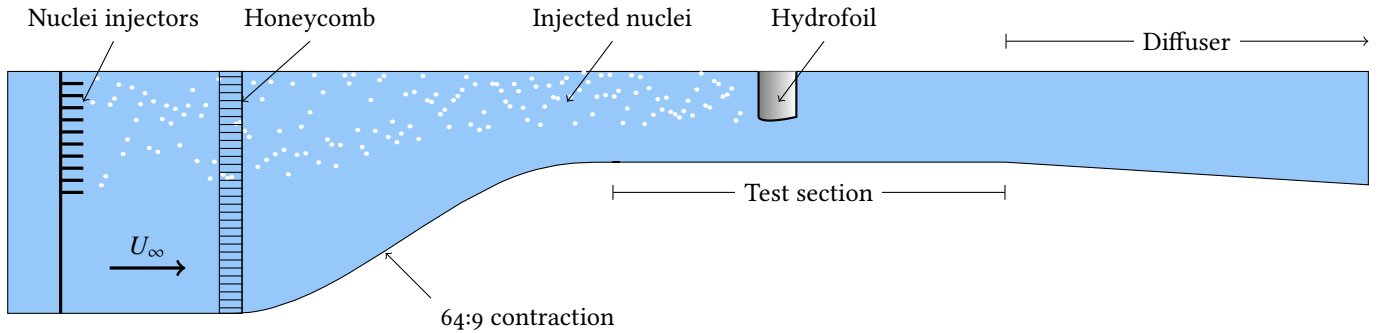


Figure 1. Tunnel schematic showing the experimental layout including the microbubble nuclei injection, contraction, test section, and diffuser.

number as $Re = U_\infty c / \nu$, where p_∞ is the static pressure at the test section centreline, p_v is the vapour pressure, ρ is the water density, U_∞ is the test section velocity, c is the chord and ν is the kinematic viscosity of the water. The freestream velocity was approximately 10.3 m/s. Two seeding conditions were investigated where the freestream is either deplete or seeded with an abundance of nuclei. For the deplete case no nuclei are injected such that only background nuclei are present in the tunnel water which do not provide active nuclei in the freestream for this flow condition [24]. For the abundant case poly-disperse nuclei with a dominant size of 10 to 15 μm are injected at a concentration of about 100 / cm^3 [25]. This volumetric concentration results in an area concentration of activated nuclei of approximately 1 nuclei / cm^2 on the hydrofoil. In both cases the tunnel water was maintained at a dissolved O_2 level of 3 ppm.

Simultaneous measurements were made of hydrofoil normal force and high-speed photography of cavitation taken from the side of the test section normal to the flow direction. The high-speed photography was recorded using a LaVision HighSpeedStar8 at a resolution of 1024×1024 pixels using a Nikkor f/1.4 50 mm lens. Simultaneous forces and high-speed images were recorded at 7 kHz for 3 s. Long-time series measurements of force for obtaining high-resolution spectra were recorded at 1 kHz for 240 s giving about 5,000 cycles of the dominant frequency. Power Spectral Density (PSD) were derived using the Welch estimate of the PSD [26] with a window size of 4096 points (4.1 s) and overlap between windows of 256 points (0.26 s). Time series of measured side force and local pixel intensity from high-speed imaging are compared to gain insight into the phasing of shed structures and the forces produced.

3. RESULTS AND DISCUSSION

A sequence of extracted images through one shedding cycle from the high-speed photography for the nuclei deplete and nuclei abundant cases are shown in figure 2. For both cases the shedding was highly periodic as can be seen from the time series of the measured lift (figure 3) and PSD of the side force (figure 4). The third PSD shown in figure 4 is for the non-cavitating case to distinguish the balance/hydrofoil response

to turbulent excitation from that due to cavitation dynamics. Additional frequency analysis beyond the PSD was carried out using continuous wavelet transforms of forces and fast Fourier transform (FFT) analysis of every pixel from the high speed photography. These analyses enabled discrimination of the peaks of the PSD between those actually associated with cavitating flow physics and those being artefacts of the FFT process. That is, wavelet transforms correlate all variations over the range of time and frequency scales investigated avoiding harmonic peaks. Amplitudes of all peak frequencies can also be mapped from FFTs of the high-speed photography to highlight regions of maximum variation or energy for each frequency to reveal which mechanisms are associated with which frequencies. Full details of these analyses are provided in a companion full length journal article in preparation.

For the nuclei deplete case, the high-speed imaging and unsteady force measurements show the dominant frequency to be $St = 0.28$ which is the second peak evident on the PSD. The analysis described above show this frequency to be associated with shedding involving large-scale cavity growth and collapse/condensation. Large-scale in this case refers to shedding involving cavity growth and collapse ranging over almost the full chord and through the midspan extending some one-half to two-thirds of the span. The first frequency peak at $St = 0.14$ can be shown to be associated with local shedding from the cavity end near the hydrofoil tip. The first frequency peak is half that of the fundamental and from the above described analyses and chordwise/spanwise space-time plots it can be shown that the strength of the local tip shedding varies at half the frequency of the bulk cavity shedding. That is, there are two separate but coupled shedding regions through the midspan and near the tip. The third peak on the PSD at $St = 0.55$ is also present at the tip when the cavity sheds sometimes at twice the frequency of the fundamental.

As a result of the above described shedding behaviour, the cavity physics and topology are complex and highly three-dimensional. Since the large-scale shedding occurs over the mid-half to two-thirds of the span it is only in this region that the cavity growth and collapse oscillations occur from the hydrofoil leading to trailing edges. As a result of this topol-

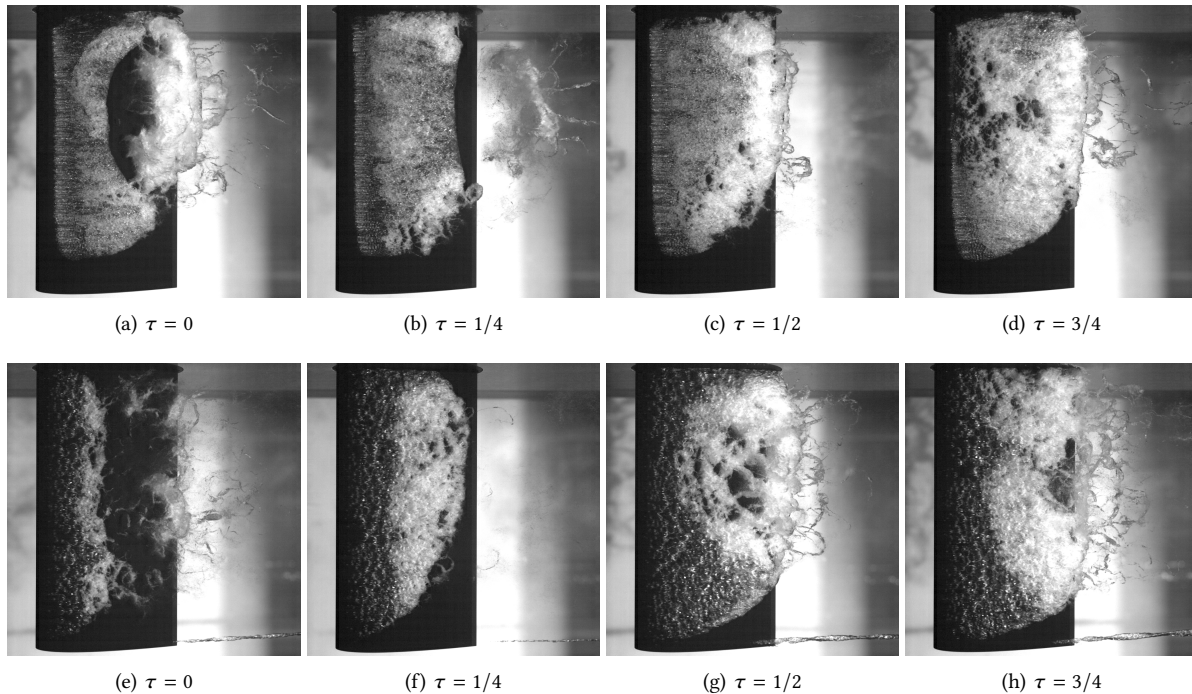


Figure 2. Photographs at one-quarter increments of the shedding cycle for the nuclei deplete (top) and abundant (bottom) conditions. Note that the shedding cycle for the deplete case is 1.8 times faster than with abundant nuclei.

ogy the cavity has a crescent shaped appearance during the growth phase (figure 2a) while the cavity regrows midspan from the leading edge. The cavity growth at midspan is much faster than that near the root and tip, quickly reaching the trailing edge (figure 2b,c) triggering a shockwave that propagates upstream. This shockwave is focused as it travels upstream due to shockwaves that form simultaneously at the root and tip travelling in the spanwise direction toward midspan. This focusing condenses the cavity through the mid span region (figure 2d) such that the cavity has to grow anew leading to the crescent shape described above. During the growth phase the cavity forms a re-entrant jet, the leading edge of which remains almost stationary as the trailing edge of the growing cavity reaches the hydrofoil trailing edge. Although the re-entrant jet may occasionally break through the surface of the growing cavity it does not initiate a shockwave as has been observed for flows about bodies with much greater adverse pressure gradients [17]. In addition to the strength of the local tip shedding varying at half the fundamental frequency, it can also be shown that the bulk shedding cavity growth rates and inter-cavity time between growth phases also vary at this lower frequency.

With an abundance of nuclei, the shedding physics were significantly altered due to the high concentration of continuously activated nuclei. The fundamental frequency of the bulk shedding was $St = 0.15$, corresponding to the first peak in the force PSD (figure 4). This shedding was approximately two-dimensional, occurring over the full hydrofoil span, and was 1.8 times slower than the large-scale shedding for the nuclei deplete case. The second peak in the PSD is twice that

of the fundamental ($St = 0.31$) and can be shown to be associated with the propagation of the first of two shockwaves each cycle. The first shockwave forms once the growing cavity reaches the trailing edge. This shockwave propagates upstream (figure 2g) but loses strength and speed, stalling before reaching the cavity leading edge. Shortly after this another shockwave forms that travels upstream with greater strength and velocity (figure 2h) causing large scale condensation with subsequent near-2D re-growth along the hydrofoil span. Due to the continuous supply of activated nuclei there is no clear cavity detachment line but a discontinuous cavity leading edge. Due to the discontinuous nature of the cavity leading edge and the continuous supply of activated nuclei the cavity is not condensed completely each shedding cycle as was the case for the nuclei deplete case. Nuclei activated at the hydrofoil leading edge grow as they are advected downstream merging to form a contiguous cavity volume. During the growth phase, advected bubbles reach the cavity trailing edge and condense simultaneous with the formation of re-entrant flow as evidenced by the lighter regions along the cavity trailing edge (figure 2e). Cavity growth is due to the volume of activated nuclei being greater than the condensing volume at the cavity trailing edge. As described above, once the slow growing cavity reaches the trailing edge, the first shockwave is initiated. As with the nuclei-deplete case the re-entrant jet apparently has no direct influence on the shedding. The peaks at higher frequencies can be shown to be harmonic artefacts of the FFT process.

With the addition of seeding, the lift coefficient dropped by 16% from 0.33 to 0.28. The drag coefficient remained

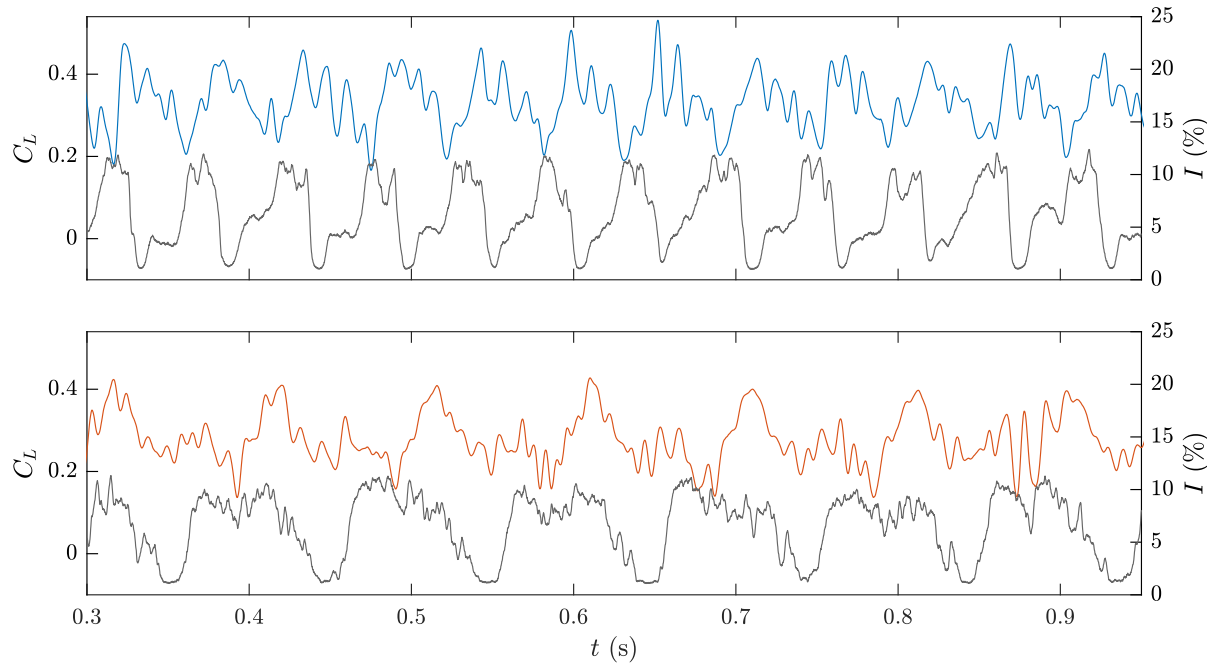


Figure 3. Time series of the lift coefficient (blue and red) and image intensity from the high-speed movies in the shedding zone (gray) for the deplete (top) and abundant (bottom) cases.

unchanged at 0.06. The fluctuating component of the lift coefficient was 0.067 for the deplete case, decreasing to 0.059 with the addition of nuclei.

4. CONCLUSIONS

The dynamics of cloud cavitation about a hydrofoil have been shown to be significantly affected by free steam nuclei content for otherwise identical flow conditions. The two bounding cases considered: nuclei deplete where there are essentially no active free freestream nuclei, and nuclei abundant where there is a large concentration of active nuclei, develop different mechanisms that lead to instability and shedding. For both cases there are two shedding modes of different frequencies but in each case the high mode frequency is a multiple of the low mode. For the nuclei deplete case the dominant mode corresponding to large-scale shedding is the high-frequency mode. The lower frequency mode being due to the variation on every alternate high mode cycle of the strength of local shedding at the cavity end near the hydrofoil tip. For the nuclei abundant case the dominant mode corresponding to large-scale shedding is the low frequency mode which is 1.8 times slower than the dominant mode for the nuclei deplete case. The high frequency mode for the seeded case is due to the propagation of the first of two shockwaves, the passage of which only partially condenses the cavity. The second shockwave condenses a much larger region of the cavity after which there is re-growth to begin another shedding cycle.

ACKNOWLEDGEMENTS

This project was supported by the University of Tasmania, the Defence Science and Technology Group and the US Office of Naval Research (Dr. Ki-Han Kim, Program Officer) and ONR Global (Dr. Woei-Min Lin) through NICOP S&T Grant no. N62909-15-1-2019.

REFERENCES

- [1] J. Franc and J. Michel. *Fundamentals of Cavitation*. Fluid Mechanics and its Applications. Kluwer Academic Publishers, Dordrecht, 2004.
- [2] Y. Kawanami, H. Kato, H. Yamaguchi, M. Tanimura, and Y. Tagaya. Mechanism and control of cloud cavitation. *Journal of Fluids Engineering*, 119(4):788–794, 1997.
- [3] M. Kjeldsen, R. E. A. Arndt, and M. Effertz. Spectral characteristics of sheet/cloud cavitation. *Journal of Fluids Engineering*, 122(3):481–487, 2000.
- [4] O. Coutier-Delgosha, B. Stutz, A. Vabre, and S. Legoupil. Analysis of cavitating flow structure by experimental and numerical investigations. *Journal of Fluid Mechanics*, 578:171–222, 2007.
- [5] H. Ganesh, J. Wu, and S. L. Ceccio. Investigation of cavity shedding dynamics on a naca0015 hydrofoil using time resolved x-ray densitometry. In *31st Symposium on Naval Hydrodynamics*, page Paper 94, Monterey, CA, USA, 11–16 September 2016.
- [6] R. Fortes-Patella, O. Coutier-Delgosha, J. Perrin, and J.L. Reboud. Numerical model to predict unsteady cavitating

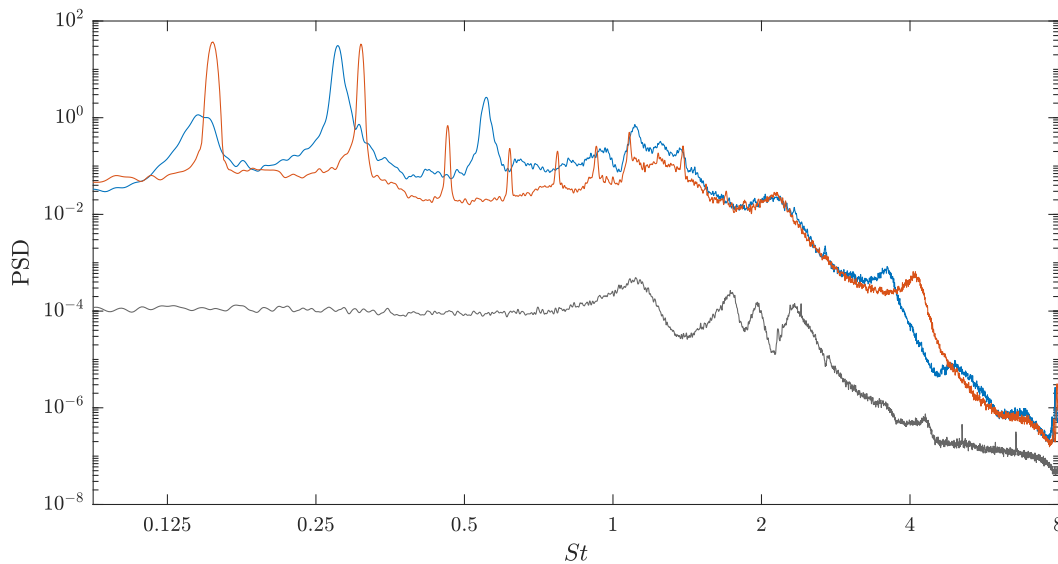


Figure 4. Power spectra of the normal force for the hydrofoil under two nuclei conditions: deplete (blue) and abundant (red). Freestream conditions are $Re = 1.4 \times 10^6$ and $\sigma = 0.55$. The foil is at a 6° angle of attack. The single-phase (non-cavitating) spectra is given in gray.

- flow behavior in inducer blade cascades. *Journal of Fluids Engineering*, 129(1):128–135, 2007.
- [7] D. Tan, Y. Li, R. Miorini, E. Vagnoni, I. Wilkes, and J. Katz. Role of large scale cavitating vortical structures in the rotor passage of an axial waterjet pump in performance breakdown. In *30th Symposium on Naval Hydrodynamics*, Hobart, Australia, 2-7 November Year.
- [8] B. Stutz and S. Legoupil. X-ray measurements within unsteady cavitation. *Experiments in Fluids*, 35(2):130–138, 2003.
- [9] A. Danlos, J.-E. Méhal, F. Ravelet, O. Coutier-Delgosha, and F. Bakir. Study of the cavitating instability on a grooved venturi profile. *Journal of Fluids Engineering*, 136(10):101302, 2014.
- [10] P. Koukouvinis, N. Mitroglou, M. Gavaises, M. Lorenzi, and M. Santini. Quantitative predictions of cavitation presence and erosion-prone locations in a high-pressure cavitation test rig. *Journal of Fluid Mechanics*, 819:21–57, 2017.
- [11] A. Gnanaskandan and K. Mahesh. Large eddy simulation of the transition from sheet to cloud cavitation over a wedge. *International Journal of Multiphase Flow*, 83:86–102, 2016.
- [12] L. Barbaca, B. W. Pearce, and P. A. Brandner. Experimental study of ventilated cavity flow over a 3-d wall-mounted fence. *International Journal of Multiphase Flow*, 97:10–22, 2017.
- [13] S. L. Ceccio and C. E. Brennen. Dynamics of attached cavities on bodies of revolution. *Journal of Fluids Engineering*, 114(1):93–99, 1992.
- [14] P. A. Brandner, G. J. Walker, P. N. Niekamp, and B. Anderson. An experimental investigation of cloud cavitation about a sphere. *Journal of Fluid Mechanics*, 656:147–176, 2010.
- [15] A. Gnanaskandan and K. Mahesh. Numerical investigation of near-wake characteristics of cavitating flow over a circular cylinder. *Journal of Fluid Mechanics*, 790:453–491, 2016.
- [16] H. Ganesh, S. A. Mäkiharju, and S. L. Ceccio. Bubbly shock propagation as a mechanism for sheet-to-cloud transition of partial cavities. *Journal of Fluid Mechanics*, 802:37–78, 2016.
- [17] K. L. De Graaf, P. A. Brandner, and B. W. Pearce. Spectral content of cloud cavitation about a sphere. *Journal of Fluid Mechanics*, 812:R1, 2017.
- [18] K. R. Laberteaux and S. L. Ceccio. Partial cavity flows. part 2. cavities forming on test objects with spanwise variation. *Journal of Fluid Mechanics*, 431:43–63, 2001.
- [19] N.-X. Lu, R. E. Bensow, and G. Bark. LES of unsteady cavitation on the delft twisted foil. *Journal of Hydrodynamics, Series B*, 22(5 (Supplement 1)):784–791, 2010.
- [20] B. Ji, X. Luo, Y. Wu, X. Peng, and Y. Duan. Numerical analysis of unsteady cavitating turbulent flow and shedding horse-shoe vortex structure around a twisted hydrofoil. *International Journal of Multiphase Flow*, 51:33–43, 2013.
- [21] B. Gindroz and M. L. Billet. Influence of the nuclei on the cavitation inception for different types of cavitation on ship propellers. *Journal of Fluids Engineering*, 120(1):171–178, 1998.

- [22] K. L. de Graaf, B. W. Pearce, and P. A. Brandner. The influence of nucleation on cloud cavitation about a sphere. In *Sixteenth International Symposium on Transport Phenomena and Dynamics of Rotating Machinery - ISROMAC16*, 2015.
- [23] P. A. Brandner, B. W. Pearce, and K. L. de Graaf. Cavitation about a jet in crossflow. *Journal of Fluid Mechanics*, 768:141–174, 2015.
- [24] J. A. Venning, M. T. Khoo, B. W. Pearce, and P. A. Brandner. Background nuclei measurements and implications for cavitation inception in hydrodynamic test facilities. Under consideration for publishing in *Experiments in Fluids*, 2018.
- [25] D. R. Giosio, B. W. Pearce, and P. A. Brandner. Influence of pressure on microbubble production rate in a confined turbulent jet. In Greg Ivey, Tongming Zhou, Nicole Jones, and Scott Draper, editors, *20th Australasian Fluid Mechanics Conference*, page Paper 717, Perth, Australia, 5-8 December Year. AFMS.
- [26] P. D. Welch. The use of fast fourier transform for the estimation of power spectra: A method based on time averaging over short, modified periodograms. *IEEE transactions on Audio and Electroacoustics*, 15(2):70–73, 1967.